

An optical spectroscopic H-R diagram for low-mass stars and brown dwarfs in Orion

F. C. Riddick^{1,2}, P. F. Roche², P. W. Lucas³,

¹ *Dept. of Astronomy & Astrophysics, Penn State University, 525 Davey Lab, University Park, PA 16802, USA*

² *Astrophysics, University of Oxford, Dept of Physics, DWB, Keble Road Oxford OX1 3RH, UK*

³ *Centre for Astrophysics, University of Hertfordshire, College Lane, Hatfield, Herts, AL10 9AB, UK*

Accepted XX Received 2007 XX; in original form 2007 April XX

ABSTRACT

The masses and temperatures of young low mass stars and brown dwarfs in star-forming regions are not yet well established because of uncertainties in the age of individual objects and the spectral type–temperature scale appropriate for objects with ages of only a few Myr. Using multi-object optical spectroscopy, 45 low-mass stars and brown dwarfs in the Trapezium Cluster in Orion have been classified and 44 of these confirmed as bona fide cluster members. The spectral types obtained have been converted to effective temperatures using a temperature scale intermediate between those of dwarfs and giants, which is suitable for young pre-main sequence objects. The objects have been placed on an H-R diagram overlaid with theoretical isochrones. The low-mass stars and the higher mass substellar objects are found to be clustered around the 1 Myr isochrone, while many of the lower mass substellar objects are located well above this isochrone. An average age of 1 Myr is found for the majority of the objects. Assuming coevality of the sources and an average age of 1 Myr, the masses of the objects have been estimated and range from 0.018–0.44 M_{\odot} . The spectra also allow an investigation of the surface gravity of the objects by measurement of the sodium doublet equivalent width. With one possible exception, all objects have low gravities, in line with young ages, and the Na indices for the Trapezium objects lie systematically below those of young stars and brown dwarfs in Chamaeleon, suggesting that the 820 nm Na index may provide a sensitive means of estimating ages in young clusters.

Key words: stars: low-mass, brown dwarfs – stars: formation – stars: pre-main-sequence – Hertzsprung-Russell (HR) Diagram

1 INTRODUCTION

1.1 Background

There has been enormous progress in brown dwarf (BD) research in the decade since the discovery of the first confirmed BDs and substellar objects have been discovered in their hundreds, both as single and multiple objects, as companions around stars in the local neighbourhood, in nearby open clusters, in star-forming regions (SFRs) and in major deep imaging surveys.

Open clusters provide the great opportunity to study properties of a large group of objects with known age, metallicity and distance. The Trapezium Cluster, the inner 0.3 pc or 2 arcmin of the Orion Nebula Cluster (ONC) (Herbig & Terndrup, 1986), is an ideal site for the study of star formation and that of low-mass stars and substellar objects

in particular. Its extreme youth (~ 1 Myr: see the discussion in section 6.1) enables the detection of the full mass spectrum down to very low mass objects, since they are substantially brighter than older objects of similar mass: according to model evolutionary tracks (e.g. Burrows et al. 1997) they are 3 orders of magnitude more luminous at an age of a few million years than they are at a few billion years. The cluster is also extremely richly populated and compact: the total membership of the ONC is 3500 stars and the total mass contained is $1800M_{\odot}$ (O’Dell, 2001). Its very high central density of $\sim 2 \times 10^4$ stars per cubic parsec (Hillenbrand & Hartmann, 1998) allows photometry of several hundred sources in relatively small surveys (e.g. Hillenbrand 1997, Lucas & Roche 2000, hereafter LR00) and makes it an ideal site for multi-object spectroscopy. The dense, dusty obscuring OMC-1 cloud ensures that background stars should

appear only at very large reddenings (e.g. Hillenbrand & Hartmann 1998), and therefore most of the stars that appear associated with the ONC really are so. In addition, its proximity allows the detection of low-mass objects and also ensures that foreground contamination is low. The high galactic latitude ($b = -19$ deg) also minimises non-member contamination. The distance to Orion KL was measured at 437 ± 19 pc by Hirota et al. from the annual parallax of water maser emission, while most estimates of the distance to the Trapezium cluster lie in the range 400 – 480 pc. In this paper we adopt a distance of 450 pc.

Confirmation of substellarity, i.e. a mass below $0.075 M_{\odot}$, is non-trivial since the spectral type of an object at the transition from stellar to substellar status (as well as that at the deuterium burning threshold) depends on the age of the object. Since BDs have no long-lasting source of fuel, deuterium-burning being relatively rapid, most of their evolution is dominated by a long, slow cooling process and they evolve through a series of spectral types as they cool, the types becoming later with age, so that a spectral type cannot be associated with a specific mass, unless the age of an object is known. This may be so in a cluster if an average age can be assumed and assigned to all members.

While photometric data yield estimates of effective temperature (T_{eff}) and luminosity, spectroscopy allows an independent and hopefully much better estimate of T_{eff} , and may provide indications of the surface gravity, crucial for providing evidence of cluster membership (see Section 4). Spectroscopy may provide evidence of the presence of circumstellar disks which in turn indicate youth and hence membership of the cluster. If membership of a cluster can be confirmed for an object then the cluster age and distance can be assigned to it and the validity of young theoretical isochrones can be tested and the spectra can be used to test and improve model atmospheres.

There are limitations however: while optical spectroscopy provides the best studied sets of spectral lines for classification, the visual extinction in a SFR severely limits the number of young BDs that can be observed in the far red optical spectral region. Additionally, comparisons between observations and models for young objects in SFRs are more uncertain because of the large amount of extinction due to the surrounding dust which modifies both the intrinsic magnitude and the colours and affects the spectra.

The aim of this project is to classify a large sample of low-mass stars and BDs in the Trapezium Cluster in Orion by an analysis of their red optical spectra using the methods of Riddick, Roche & Lucas (2007; hereafter Paper I). The spectral types are converted to T_{eff} by the use of a suitable temperature scale, which allows an estimate of the average age of the cluster, by a comparison with theoretical evolutionary tracks on a Hertzsprung-Russell diagram (HRD). Under the assumption of a coeval population, masses will be estimated.

1.2 Outline

In Section 2 we describe the data selected for observation, the experimental setup, the slit mask design, the observations and data reduction, including dereddening and nebular emission subtraction. In Section 3 the classification is carried out according to the procedures described in Paper I.

In Section 4 the membership probability of the objects is determined, also using the procedures described in Paper I. In Section 5 the HRD is constructed, including the conversion of spectral type to temperature using an appropriate temperature scale. In Section 6, the HRD is analysed and compared with other studies. In Section 7, we will summarise the results.

2 OBSERVATIONS IN THE TRAPEZIUM CLUSTER

Observations were conducted on the 3.9m Anglo-Australian Telescope (AAT) using the Taurus focal reducer in multi-object spectroscopic mode and on the 8.0m Gemini-North telescope where the Gemini Multi-Object Spectrograph (GMOS) was used. Time was awarded for four separate observing runs for the spectroscopy, two on each telescope. The observations are summarised in Table 1.

2.1 Selection of Targets

The target objects for spectroscopy were chosen from the IJH survey of LR00 and from the JHK survey of Lucas et al. (2005). Targets were selected in areas away from the cluster's very bright nebulous core, to enable on average fainter objects to be observed in regions of lower background emission.

Objects were chosen with magnitudes in the range $H=11-18$, i.e. from low-mass stars down to planetary-mass object (PMO) candidates, but with most targets close to the H-burning limit at $H \sim 13.5$ mag for lightly reddened objects. For all runs, sources were selected preferentially if they had low extinction, with $A_V < 5$, though some sources with higher extinction were included to fill in space in the masks which could not be filled by low-extinction objects. Several of the objects were observed through more than one mask and/or on more than one run to fill up available space, allowing a limited study of variability in a few of the objects – see Section 3.3. The faintest objects included in the masks yielded spectra with insufficient signal to noise ratio (S/N) to allow classification, so for the second runs at each telescope all but the brightest PMO candidates were excluded.

2.2 Slit Masks

To maximise the number of objects observed, slit heights in the multi-object slit masks were 5-7 arcsec – the minimum sufficient to allow the spectra at the two telescope nod positions to lie within the height of the slits. Short nods (3-4 arcsec) were used to minimise the difference in nebular background after subtraction of neighbouring image pairs. The AAT masks each contained 30-32 slitlets and the GMOS masks 23-26.

2.3 AAT Observations using Taurus

The AAT observations were carried out by FCR and PWL using Taurus++ at the f/8 Cassegrain focus of the telescope. The field in the vertical direction was 8.4 arcmin with a scale

Table 1. Observation Log

Telescope	Dates (2002)	Instrument	Exposure Time (mins)	Slit Width (arcsec)	Telluric Standards
AAT	Jan20	Taurus	60,20,15	1.5	w485a
AAT	Dec 27-29	Taurus	340,220	1.3	HD84937
Gemini-N	Mar (8 nights)	GMOS	240,200	0.8	Feige 34
Gemini-N	3,8,9,10 Nov; 2 Dec	GMOS	240,120	0.8	GD71, HZ2

of 0.37 arcsec/pixel. A red volume phase holographic grating dispersed the light from multi-slit masks inserted at the telescope focal plane. An OG515 filter was used to avoid second order contamination of the spectra. The detectors used were MITLL2A and MITLL3A for the 1st and 2nd runs respectively. Spectral coverage was 6000–10,000 Å for objects located within the central 2 arcmin of the field in the dispersion direction, with reduced spectral coverage for objects located towards the edges. The resolving power employed was $R \sim 1000$, sampled at 2.8 Å/pixel.

Taurus was used in ‘nod and shuffle’ mode (Bland-Hawthorn & Jones 1998; Glazebrook & Bland-Hawthorn 2001), the major advantage of which is extremely accurate subtraction of night sky emission in spectroscopy, since OH airglow changes on short timescales of a few minutes. It allows relatively rapid nodding of the telescope, providing good subtraction of the airglow lines with no penalty of multiple CCD readouts, resulting in a high observing efficiency. In this case, cycles of 1 minute were used.

Nod and shuffle did work very well for the subtraction of the spatially uniform though temporally variable terrestrial sky background but it could not completely subtract the highly spatially structured nebular background, which varies on spatial scales smaller than the nod length used. The nebular spectrum, therefore, still often appeared as a series of lines in emission or absorption, depending on the local gradient in the extracted spectra. This is especially true for $H\alpha$ emission, which was present and strong in all the spectra.

Due to their intrinsic faintness, acquisition of the targets was not easy. Stability problems in the mask wheel (not rotating to exactly the expected positions) and a lack of suitable astrometric software made it very difficult to acquire the masks and for the first run only one mask was able to be observed for the full hour intended and only 3 masks were used in total, due in addition to time lost to poor weather. It was decided to observe only one mask on each night of the second run to minimise the acquisition overheads.

2.4 Gemini-North Observations using GMOS

GMOS on Gemini-North was used for multi-object spectroscopy, providing a 5.5 arcmin FOV. The R400 grating was used, giving spectral coverage from 6000–10,000 Å and a spectral resolving power of $R \sim 2000$ and a sampling of ~ 0.7 Å/pixel. The observations were carried out by observatory staff. The detector consisted of 3 CCDs each of size 2048x4608 pixels, i.e. a total of 6144 x 4608 pixels in the spectral and spatial directions respectively, with a scale of 0.073 arcsec per pixel; see table 1. Nod and shuffle was not available on GMOS and sky correction relied on subtraction from the nodded position.

2.5 Data Reduction

The data were reduced using standard procedures within IRAF. Dispersed images were coadded before sky subtraction and extraction. The data were bias corrected, flat-fielded and corrected for telluric absorption. A telluric standard was observed on each run, to allow the spectra to be corrected for atmospheric absorption features. Telluric bands should not present significant problems with spectral typing (e.g. Kirkpatrick et al. 1991), and the typing procedure used was designed to be relatively unaffected by the presence of telluric absorption. Observations of standard stars were undertaken at similar airmasses to the average of those for the science observations. CuAr arc lamp spectra were obtained and used for wavelength calibration, typically accurate to 0.5 pixel.

2.5.1 Nebular Emission Line Extraction

Nebular line subtraction is necessary since a significant source of noise arises from the spatial gradients in the nebular emission, which makes background subtraction problematic. We fit a polynomial to the residual background at each wavelength and subtracted this during the extraction, as done by Lucas et al. (2001, hereafter LR01). This was partially successful in removing nebosity gradients (and residual OH emission), but it is not a perfect correction in most cases and nebular lines are still seen in many of the spectra even after sky subtraction. It is worst for the faintest sources which have peak brightness comparable to nebular surface brightness fluctuations on a scale of a few arcsec even in low background regions.

2.5.2 Dereddening of Spectra and Fluxes

In a young cluster such as Orion, it is necessary to correct for differential reddening towards individual stars since the extinction varies on small scales due to the highly structured nebosity. The DEREDDEN task in IRAF was used to deredden the spectra to the theoretical NextGen (J-H) vs H colour-magnitude sequence of Baraffe et al. (1998; BCAH98 hereafter) at age 1 Myr. The reddening parameter was set at the typical interstellar value of $R_V = 3.1$ since this produces very similar extinction values to the Rieke & Lebofsky (1985) extinction law, which appears to be suitable for the Trapezium cluster (Lucas et al. 2005).

Uncertainties in A_V of ± 1 mag are expected due to photometric errors and since many of the young sources may have IR colours affected substantially by emission from circumstellar disks and envelopes (Luhman & Rieke, 1999). Objects with negative derived extinction estimates are given a value of zero.

The procedure used for spectral typing was designed to

ensure that the results are relatively immune to the effects of reddening on the spectra and, as described in Paper I, errors in reddening corrections are likely to give errors in the spectral type of typically less than 0.1 subtypes.

3 SPECTRAL CLASSIFICATION

Young, low-mass objects are located on primarily vertical tracks on the HRD (e.g. BCAH98) therefore mass estimates are much more sensitive to errors in temperature than luminosity. Temperature is derived from the spectral type so it is crucially important to assign spectral types as accurately as possible. To this end, we devised in Paper I a classification system valid for the spectral range M3-M9 and independent of both reddening and nebular emission lines and we have used this system to classify these data. Specifically, we employed the indices recommended in paper I, sampling the spectra near 7445, 8000, and 8440 Å using the VO 7445 index defined by Kirkpatrick et al (1991), the VO 2 index of Lepine et al (2003), and the c81 index of Stauffer et al (1999).

3.1 Spectral Types Assigned

Following the spectral typing, 45 of the objects observed were able to be assigned a spectral type – see Table 2. An additional 11 spectra were untypable due to low S/N or veiling but appeared to have M type features – see Table 3. The observed and dereddened fluxes given in Table 2 use data from the UKIRT IJH photometry of LR00 and LR01 where good quality data are available, since these fluxes were obtained almost simultaneously. Fluxes from the Gemini data of Lucas et al. (2005) were used otherwise, except in the case of 148-831 (2MASS J05351475-0528318) where the only available data was the 2MASS fluxes. We note that the dereddened UKIRT H band magnitudes used in the H-R diagrams agree with the Gemini data (within the error bars) in the great majority of cases. The spectral types given by the indices are listed in the Appendix, but the final class assignments were done manually for this sample to ensure that spurious results were not introduced by nebular contamination. The spectra of all of the objects successfully extracted are shown in Figure A-1 in the Appendix and the final spectral classes assigned are listed in table 2. Comparison with the types listed in the Appendix demonstrates that the final classes are generally consistent with those given by the indices within the estimated uncertainties, although in a few objects the indices give significantly different classes, demonstrating that using several indices covering a range of spectral features is desirable, in addition to an independent classification by comparison with other classified objects.

The names of the objects are derived from the coordinates, following the convention of O’Dell & Wen (1994): the first 3 (or 4) digits are RA offset from 05 hours, 35 minutes and the last 3 (or 4) digits are declination offset from -05 degrees, 20 minutes. For example, object 084-305 has RA = 05:35:08.4 and Dec = -05:23.05. 2MASS was used to

calibrate the astrometry from the photometric surveys. The coordinate based names used in LR00 and LR01 sometimes differ slightly from those used here, since these were based on a less accurate astrometric calibration. For clarity, Table 2 also includes the names used in those publications (ID LR00) and the running number used in Lucas et al. (2005) is also given (ID LRT05).

3.2 Veiling

Robberto et al. (2004) find that since the ratio between the accretion luminosity and the total stellar luminosity, corresponding to the veiling factor of the stellar absorption lines, is generally small, the positions of the stars in the H-R diagram remain almost unaffected by the removal of any accretion contribution. Veiling of narrow absorption lines can be high if hot gas in a stellar wind produces an emission line that veils the stellar absorption line, but this is likely to be less problematic for broad molecular bands.

Veiling in a spectrum from either dust scattering or circumstellar emission can reduce the contrast of molecular absorption bands and make a later type spectrum look like an earlier type. The effect is typically less than 1.5 subtypes (Hillenbrand 1997), but can occasionally be much larger. A number of objects in this sample display emission in the Ca II triplet lines indicative of emission from circumstellar material, which could dilute molecular features. In most cases, any veiling appears to be weak, but in two of the objects that could not be classified, the effect is prominent. These objects are described in section 4.2 and the effects are discussed in section 6.3.

3.3 Comparison of Spectral Types from Different Runs

To investigate variability of the objects and to check on the accuracy of spectral types obtained, we compared the spectral types obtained from different runs and found them to be generally in extremely good agreement – see Table 4. Where the types do not agree, the types obtained from the GMOS runs were usually used for the final spectral type due to the higher S/N and resolution, but this was decided on a case by case basis. The largest difference in spectral type for multiply observed objects is 0.75 subtypes and for types earlier than M6 the agreement is always within 0.5 subtypes. Since the overall spectral typing error is 0.5 subtypes and 1–2 subtypes for types earlier and later than M6 respectively, we conclude that we have not detected any significant spectral variations. Note, however, that the spectrum of the unclassified object 047-436 does show significant changes; this is discussed in the Appendix.

3.4 Completeness of Spectroscopy

To investigate the completeness of the spectroscopic sample, the observed H magnitudes of all the objects observed were plotted with respect to whether or not a spectrum was obtained in Figure 1. There is no sharp cutoff, as expected due to the very different aperture sizes and exposure times used for the 4 runs, and the variability in the nebular emission.

Table 2. Photometry & Spectral Types Assigned. Observed Cousins I band fluxes and dereddened I, J and H fluxes are given.

NAME	I_{obs}	I_{dr}	J_{dr}	H_{dr}	A(V)	Spectral Type	Type Error	ID(LR00)	ID(LRT05)
011-027	17.10	16.95	15.48	14.95	0.3	3.25	1.0	011-029	
4584-117	15.77	13.62	12.08	11.37	3.7	3.5	0.5	4585-118	
177-541	18.97	16.79	15.24	14.70	3.8	4.25	1.5	177-540	154
112-532	16.76	14.69	12.98	12.36	3.6	4.75	0.5	112-531	171
082-403	15.95	13.59	12.23	11.53	4.1	4.75	0.5	083-403	265
091-017	16.53	16.53	14.19	13.68	0.0	5.0	0.5	091-019	
034-610	16.18	15.86	13.81	13.24	0.6	5.25	0.5	035-609	117
016-534	15.79	15.79	13.42	13.04	0.0	5.25	0.5	016-533	166
130-458	17.09	14.78	13.01	12.38	4.0	5.25	0.5	130-458	220
121-434	17.10	14.52	13.26	12.66	4.4	5.5	1.0	122-434	
017-636	16.91	14.70	13.13	12.51	3.8	5.5	1.0	017-635	79
037-246	16.94	14.97	12.33	11.63	3.4	5.5	1.0	038-246	339
222-745			15.46	14.93	2.3	5.75	0.5		2
068-019	17.11	16.76	14.28	13.73	0.6	5.75	0.5	068-020	
019-354	17.94	17.05	14.36	13.81	1.5	5.75	0.5	019-354	281
103-157	15.98	15.38	13.33	12.73	1.0	5.75	0.5	103-158	390
017-710	16.45	16.32	13.76	13.18	0.2	6.0	0.5	018-709	36
069-209	16.32	16.32	14.09	13.67	0.0	6.0	0.5	069-210	380
156-547	19.59	18.60	16.34	15.82	1.7	6.0	1.0	156-546	149
4559-109	18.85	16.79	14.34	13.79	3.6	6.25	0.5	4560-109	
102-102	16.95	16.95	14.32	13.86	0.0	6.25	0.5	102-102	
095-058	16.51	16.51	13.71	13.25	0.0	6.25	0.5	095-100	
077-453	16.23	15.11	13.36	12.76	1.9	6.5	0.5	077-452	229
072-638	18.11	17.46	15.20	14.66	1.1	6.5	0.5	073-637	70
053-503	17.46	16.25	13.64	13.06	2.1	6.5	1.0	053-503	208
154-600	16.97	16.44	13.48	12.89	0.9	6.5	0.5	154-559	132
014-413	18.40	17.47	14.71	14.16	1.6	6.5	1.0	014-413	254
4569-122	17.78	16.81	14.30	13.74	1.6	6.75	1.0	4570-123	
035-333	16.84	16.84	13.81	13.24	0.0	6.75	0.5	035-333	290
096-1943	18.78	18.07	15.29	14.75	1.2	6.75	0.5	096-1944	
055-230	17.68	17.15	13.69	13.11	0.9	6.75	1.5	055-231	358
084-305	18.01	15.70	13.12	12.50	4.0	7.0	0.5	085-305	320
030-524	20.59	20.11	17.66	17.12	0.8	7.5	1.5	031-524	178
217-653			14.52	13.97	1.7	7.75	0.5		55
042-012	18.12	17.62	14.32	13.76	0.9	7.75	1.0	043-014	
092-606	20.74	19.90	16.68	16.17	1.4	8.0	2.0	092-605	122
186-631	19.54	18.84	15.60	15.07	1.2	8.0	1.0	186-631	85
130-053	20.24	19.98	15.65	15.12	0.4	8.5	2.0	131-054	
047-550	20.89	20.30	16.96	16.45	1.0	8.5	2.0	047-549	143
077-127	18.76	18.24	14.69	14.14	0.9	8.5	1.0	078-128	
082-253	19.88	18.01	15.67	15.14	3.2	8.5	1.5	083-253	332
148-831			15.53	15.00	4.8	8.5	2.0		
183-729			17.69	17.15	1.3	8.75	1.5		18
165-634	20.21	18.79	15.70	15.17	2.4	8.75	1.0	166-634	82
031-536	20.23	20.23	16.72	16.23	0.0	8.75	1.0	032-536	159

Table 3. Probable M-type Objects. These showed basic M-type characteristics but were unclassifiable due to low contrast of spectral features or low S/N.

NAME	I_{obs}	I_{dr}	J_{dr}	H_{dr}	A(V)*	Spectral Type	ID(LR00)	ID(LR05)	Notes
117-609			10.08	9.51	12.2	early-M		119	veiled,CaII
050-143	20.62	20.25	17.57	17.04	0.6	mid-M	050-144		
196-700	21.09	19.23	16.95	16.44	3.2	mid-M	196-659	47	
046-245	19.89	19.18	16.92	16.41	1.2	late-M	047-245	342	
139-425	17.65	16.55	14.49	13.94	1.9	M	140-425		
086-324	18.66	15.87	13.85	13.27	4.8	M	086-324	296	
041-210	20.55	18.23	16.12	15.60	4.0	M	042-210	379	
160-607			11.07	10.33	11.7	M		120	heavily veiled,
084-119	18.58	15.35	13.42	12.83	5.6	M?	085-121		CaII
047-436	18.28	14.67	13.85	13.28	6.2	M	047-436	242	heavy veiled, CaII
044-219		15.65	15.12		2.9	Late M			

Table 4. Comparison of Spectral Types measured on more than 1 Observing Run

ID	AAT 1	AAT 2	GMOS 1	GMOS 2	Final Type
091-017		M4.5	M5		M5
034-610	M5.25			M5.25	M5.25
121-434	M5.25			M5.75	M5.5
068-019	M5.5		M5.75		M5.75
019-354	M5.5		M6		M5.75
069-209	M5.75		M6		M6
095-058	M6		M6.25		M6.25
053-503	M6.5		M6		M6.5
072-638	M6			M6.75	M6.5
077-453	M6.25			M6.5	M6.5
014-413	M6.25	M6.25	M7		M6.5
035-333	M6	M6.25	M6.75		M6.75
084-305	M6.5	M7.5	M7.25		M7
042-012	M8.5		M7.75		M7.75

The level of completeness is approximately constant for $12 < H < 16$ mag, corresponding to approximately $0.3\text{--}0.03 M_{\odot}$. No objects were classified successfully for $H > 17.5$.

4 CLUSTER MEMBERSHIP

4.1 Gravity Sensitive Features

Young objects which are still contracting to the MS have surface gravities intermediate between those of field dwarfs and giants. There are several optical spectral features, most notably alkali metal absorption lines, which are extremely sensitive to surface gravity and hence useful indicators of age and cluster membership.

The main form of evidence of cluster membership available in these spectra is very weak Na I doublet absorption at $8183/8195 \text{ \AA}$. An analysis of this feature using the Kirkpatrick et al. (1991) C ratio was carried out in Paper I for M type objects of different surface gravities: field dwarfs, giants, dwarf/giant averages and young M type objects in the Chamaeleon I SFR (having an average age of 2 Myr). We calculated this ratio for the 45 Trapezium objects with spectral types assigned – see Figure 2.

Studies of the NaI and KI absorption lines in the near-infrared show a similar trend, with substantially lower equivalent widths in young cluster objects than in field dwarfs (e.g. Allers et al. 2007, Close et al. 2007, Gorlova et al. 2003, Luhman et al. 2007, LR01)

A deep spectrum of Orion by Osterbrock, Tran & Veilleux (1992) does not reveal any emission lines in the vicinity of the $8183/8195 \text{ \AA}$ Na doublet, indicating that the Na C gravity index is not contaminated by nebular emission lines.

The Trapezium spectra have weak Na strengths much closer to giant than dwarf values, demonstrating their youth and PMS nature. The Na index correlates with the spectral type, but the index value for one object, 183-729 (M8.75), lies above the general trend and almost overlaps with the values seen for the dwarf spectra. Examination of the spectrum shows that it does in fact have weak Na absorption

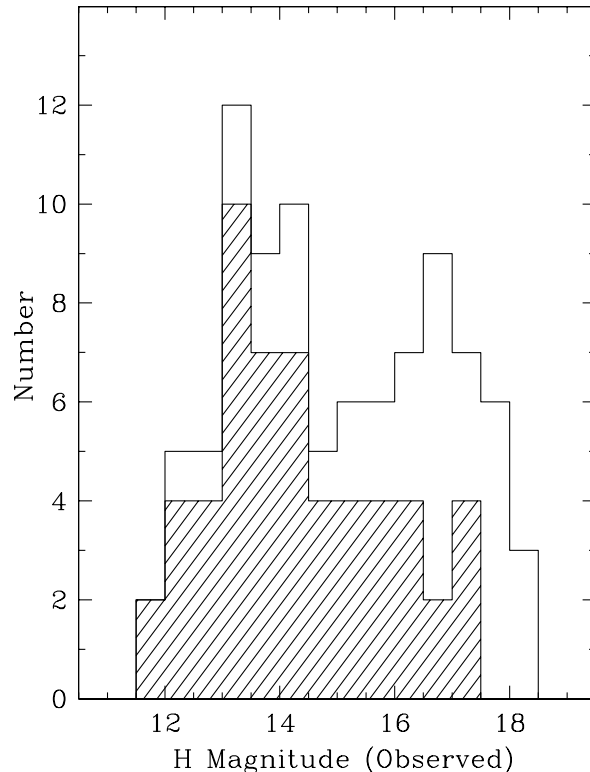


Figure 1. Histogram of H Magnitudes of Objects Observed. The shaded area represents objects whose spectra were classifiable. As expected, the number of objects observed with successful spectroscopy drops at fainter magnitudes, but even at brighter magnitudes it is not completely successful, due to the very different integration times used (and the aperture sizes) on the different runs.

and is a low gravity source and the index was affected by a negative spike in the spectrum that affects the continuum level, making the index higher than it should be. Source 011-027 (M3.25) has an index value which overlaps that of the Chamaeleon sequence, this is also very close to the dwarf sequence at these early M types. Although its Na absorption is closer to the value for a young object than a dwarf, considering the estimated error of ± 0.05 this is inconclusive. The location of this object on the HRD (Figure 4) indicates that it is underluminous for its spectral type. Its spectrum does not appear to be significantly affected by veiling as we would expect this to also weaken the Na absorption. None of the other objects have absorption as strong as that seen in the dwarf sequence indicating that they are all very likely cluster members.

Figure 3 compares the Na index values measured for the Trapezium objects to those of the Chamaeleon objects and the M standards used in Paper 1; the individual Na indices are listed in Table A.1 in the Appendix. The Trapezium objects have slightly lower values of the Na index than the Chamaeleon objects, consistently lying below them in the plot. The weaker Na absorption in the Trapezium objects indicates that they have lower surface gravity and hence are younger on average than the Chamaeleon objects. However the difference is small (compared with the difference in the index calculated for the dwarfs and giants), as expected since the average ages of the clusters are similar – 2 Myr

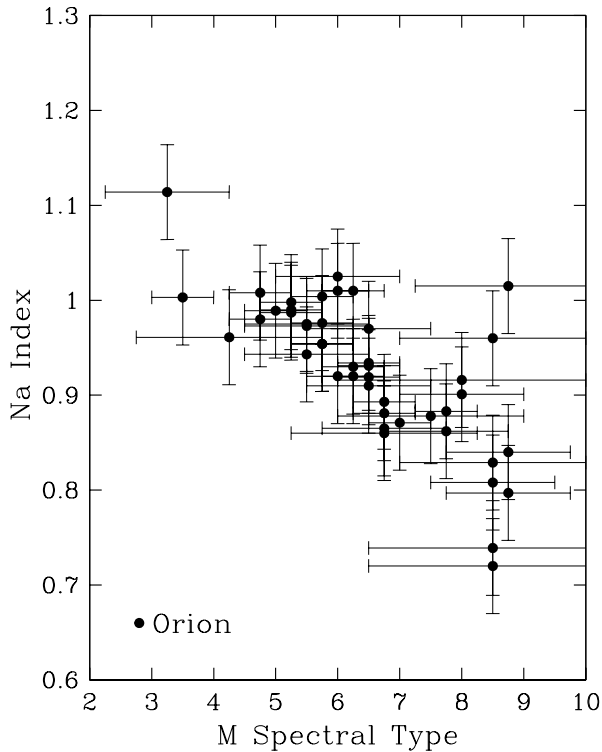


Figure 2. Variation of Kirkpatrick et al. (1991) Na Index with spectral type for Trapezium Objects.

for Chamaeleon (Luhman, 2004) and 1 Myr for the Trapezium, but does indicate that surface gravity has a relatively strong variation with age at these very young ages. This suggests that careful measurements of the Na index may be very helpful in investigating the ages of clusters and perhaps even individual objects within clusters.

In order to investigate whether the Na index can provide information on the ages of the individual Trapezium objects, the sample was divided into those lying above and below the 1Myr BCAH isochrone on the H-R diagram plotted in Figure 4 (see section 5). However, no systematic differences between the Na indices in the two groups were found, and it appears that the scatter in the Na index is due to random errors incurred with spectral typing, luminosity estimates and the calculation of the Na index itself, rather than to systematic age differences within the cluster.

4.2 Circumstellar Disks

A dusty disk surrounding an object is an indication of extreme youth and hence of cluster membership. The presence of circumstellar disks may be inferred in optical spectra by emission from the Ca II triplet lines at 8498, 8542, 8662 Å, which is a signature of a disk wind. Circumstellar Ca II line emission is detected in several of the Trapezium objects. It is prominent in the spectra of 037-246, 017-636, 121-434, and weaker in 030-524, 177-541, 095-058, and 014-413 (and also present in several of the untypable spectra, see Table 3).

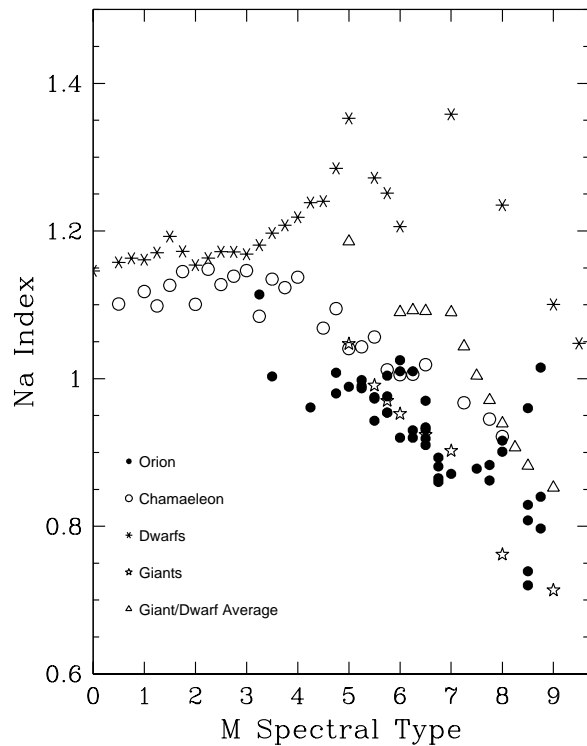


Figure 3. Kirkpatrick et al. (1991) Na Index for Trapezium Objects, Chamaeleon I Objects and M Standards. The Na index is plotted against spectral type for objects of different gravity marked by the symbols listed on the figure.

This offers additional evidence that these objects are young and hence cluster members. The equivalent widths of the λ 8498 Å Ca II line range from 24 Å in 121-434 to 3 Å in 014-413; the highest value, 36 Å, is in the untypable object 047-436 where a combination of vigorous accretion and extinction presumably combine to obscure the stellar absorption features. The spread in the spectral types given by the indices is no greater in the objects with Ca II triplet emission than the objects where Ca II emission is not detected (see Table A.1), suggesting that contamination by continuum associated with accretion does not have a significant effect on the spectral classification; this is confirmed by visible inspection and comparison with template spectra. Note that 177-541 also displays prominent emission lines at 8446, 8578 and 8729 Å which are much brighter than the Ca II triplet emission; the lines presumably arise from [O I], [Cl II] and [C I]/HeI. The [O I] and [Cl II] lines are present in the deep Orion spectrum presented by Osterbrock, Tran & Veilleux (1992), but are much brighter than the nearby Paschen H lines in 177-541, which suggests that they are associated with the star rather than just being due to residual nebular emission.

4.3 Membership Statistics

Hillenbrand & Carpenter (2000) calculated the expected foreground and background contamination in the central 5.1x5.1 square arcmin using a modified version of the Galactic star count model of Wainscoat et al. (1992) and taking into account the variable extinction across the region. This, in combination with the photometric study of Muench et al. (2002), indicates that contamination by background objects starts to become significant at $K = 16$, rising at fainter magnitudes and perhaps peaking at $K = 19-20$ (Hillenbrand & Carpenter 2000). This magnitude limit includes all the objects observed here with spectral types assigned, therefore background contamination is likely negligible, and we would expect less than one field star in the dataset of 45 spectra.

5 CONSTRUCTION OF THE HRD

In order to place an object on the HRD, its temperature must first be established, as well as either its bolometric luminosity or magnitude in a single band. If the diagram is overlaid with isochrones then the age spread of the cluster can be determined. An average age for the cluster can then be applied to all members in order to estimate their masses. Both the spectral typing and the conversion to T_{eff} are critical since a star's mass and age derived from its position on an H-R diagram is primarily a function of its assigned T_{eff} , i.e. its observed spectral type, since at these ages the objects lie on primarily vertical tracks (e.g. BCAH98; see Figure 4). Hence uncertainties in the masses derive mainly from uncertainties in the spectral types.

5.1 Dwarf, Giant and Intermediate Temperature Scales

Since evolutionary models are given in terms of T_{eff} and not spectral type, a conversion is required from the spectral types obtained from the spectra. The main difficulty with estimating ages and masses for PMS stars from the H-R diagram is the establishment of a reliable temperature scale for young T-Tauri like objects. The temperature scale for late-M dwarfs is highly uncertain (Luhman & Rieke 1998; Gorlova et al. 2003), and in particular the same spectral type will not correspond to the same temperature in a dwarf, PMS object or giant, so temperature scales have to be defined for all these luminosity classes.

For G and K stars, giants are cooler than dwarfs whereas M giants are warmer than M dwarfs for the same spectral type, the crossover being at M0 (Luhman 1999), although the magnitude of the temperature difference varies with spectral type and the scale used. The M giant scale of Luhman (1999) is warmer than the M dwarf scale by 200-400K, the difference being largest at mid-M types, where most of the data in this study lie. Hillenbrand & White (2004) find even larger differences: M2, M4 and M6 types being 310, 500 and 620K warmer for giants than dwarfs respectively. For M stars, the adoption of an intermediate temperature scale instead of one for dwarfs therefore moves the stars to older ages and higher masses on the evolutionary tracks than those obtained from using dwarf temperature scales (and more so at lower masses).

It is therefore vital to use a suitable scale for conversion and so, when choosing an appropriate temperature scale, the expected age of the objects must be taken into account. With the expected average age of the Trapezium objects being ~ 1 Myr, a dwarf scale is inappropriate due to the lower gravity of PMS stars.

5.1.1 Temperature Conversion

We have used the scale of Luhman et al. (2003b) to convert from spectral types to T_{eff} . The scale is an extension to M9 of that in Luhman (1999), which begins at M0 and ends at M7.5, using data from Taurus and IC348, following the trend for earlier types and assigning temperatures intermediate between dwarf and giant scales. This scale has been used extensively for young objects, e.g. in the Chamaeleon I region by Luhman (2004) and Neuhauser & Comeron (1999) and in Taurus by White & Basri (2003). This scale is also compatible with BCAH98 models.

The temperature difference between M8 and M9 is larger than between other subtypes. The low temperature derived for types later than M8 therefore has the effect of moving these objects to lower masses and younger ages on the HRD if this scale is correct. Note that the position of the latest spectral types on the H-R diagram is very sensitive to the temperature scale adopted.

5.2 Luminosity

Since mass estimates for young low mass stars are relatively insensitive to uncertainties in the luminosity (except at ages younger than 1 Myr), the choice of band and the calculation of luminosity is not as critical as the spectral typing and temperature conversion for the estimation of masses, although luminosity errors will affect the derived ages to a greater extent.

Synthetic colours available in evolutionary models such as those of BCAH98 provide a more accurate determination of the intrinsic properties from the observed magnitude and/or colour. These evolutionary tracks provide self-consistent flux predictions, permitting luminosity and mass to be obtained without the need for empirical bolometric corrections. This is especially advantageous for stars younger than 10 Myr since they are embedded in molecular clouds and often have excess UV (accretion) and IR (disk) emission, so the bolometric stellar luminosity cannot be derived by simply integrating the broadband photometry. To avoid contamination by these types of nonstellar emission, the luminosity must be derived using measurements at wavelengths where veiling is expected to be relatively small.

To compare the observations with models, we plot T_{eff} against the dereddened H magnitudes obtained from the photometry of LR00 and Lucas et al. (2005). Figure 4 shows the HRD for the Trapezium objects, plotted with the isochrones of BCAH98 and D'Antona & Mazzitelli (1997). The dereddened H magnitudes are converted to solar luminosities by the application of a bolometric correction which takes the form $\text{Log}(L_{\odot}) = -0.401 + 4.14(H_{\text{dered}})$ in this luminosity range at the adopted distance of 450 pc; this scale is plotted on the right hand ordinate.

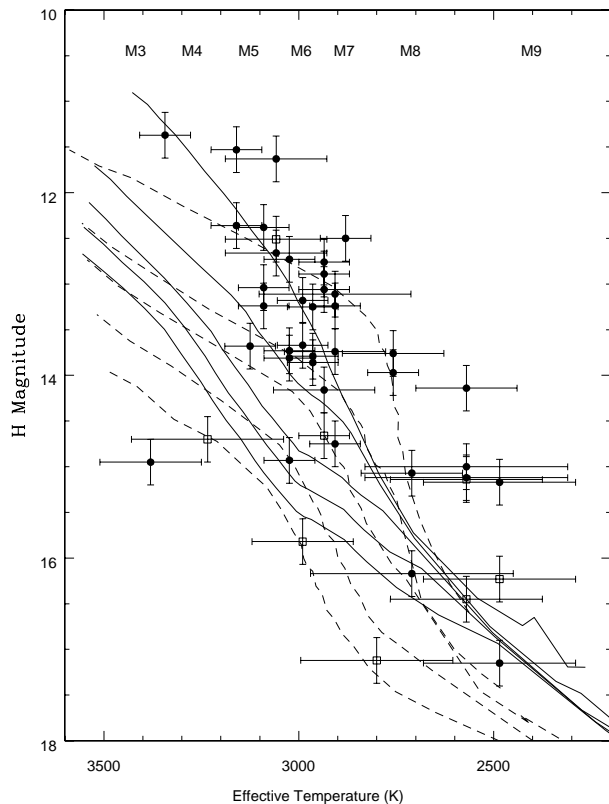


Figure 4. The Trapezium Cluster HRD. The isochrones of BCAH98 are shown for ages of 1, 3, 5, 7 and 10 Myr (solid lines, top to bottom) and those of DM97 are shown for ages of 1, 3, 5, 10 and 20 Myr (dashed lines, top to bottom). Objects which have anomalously blue colours are plotted as open squares. The origin of the error bars is described in the text. The dereddened H-magnitudes of the 45 objects which have been successfully typed are plotted on the left hand ordinate, while the total luminosity is shown on the right hand side after application of bolometric corrections.

5.3 Sources of Error on the HRD

For the majority of sources earlier than M8 the uncertainty in the spectral type is less than ± 0.5 subtypes, as shown in Table A-1. The uncertainty in temperature derived from the spectral type therefore consists of this random error in addition to any systematic error present in the temperature scale itself, e.g. due to the surface gravity not being exactly that of the average of dwarfs and giants (as discussed in Section 5.1.1).

Errors in the luminosity arise from errors in the photometry, which are typically 0.1 mag – see LR00 and Lucas et al. (2005) for a detailed discussion. We have conservatively assumed a constant 0.25 mag error to account for additional errors due to dereddening and scattered light effects in these young objects. Variability may also be present and could be quite significant; for example, Scholz & Eisloffel (2004) find several LMS and BDs in ϵ -Ori show variability attributed to rotation, accretion and flares. The spectral variability of these Trapezium sources is investigated via a comparison of the spectra between the different runs in Section 3.3 and

found to be unobservable within the estimated spectral typing errors.

5.4 Evolutionary Models

We use the Lyon Group models for the analysis of these data. The models provide mass-age-colour-magnitude relationships and are compatible with the temperature scale used. The ‘NextGen’ (BCAH98) models we use are appropriate for dust-free atmospheres at $T_{\text{eff}} > 2400\text{K}$ and are calculated using nongrey model atmospheres. There are no objects in this sample with $T_{\text{eff}} < 2400\text{K}$ and so dust formation is not likely to affect the spectra significantly. This is supported by the strength of the TiO and VO molecular bands present in all the spectra and in the values of the indices calculated (see Paper I) – they are strong in all the spectra and have not started decreasing in strength at types earlier than M9, as would be expected if dust condensation occurred.

Other models have also been produced and used widely, e.g. Burrows et al (1997; BM97) and D’Antona & Mazzitelli (1997, updated in 1998; DM97), as used by LR01 for the estimation of masses for many of the same objects.

6 ANALYSIS OF THE HRD

6.1 Ages & Star-Formation History

The technique of estimating ages and masses from the HRD by adopting an average age for the cluster has been used in a number of star formation regions, e.g. in Taurus (Briceño et al. (2002), White & Basri (2003)), in Rho-Ophiuchus (Willing et al. 1999) in NGC 2024 (Levine et al 2006), and in Orion (Slesnick et al. 2004).

Age estimates become highly uncertain at very young ages, because the state of evolution depends critically on the initial conditions. The BCAH98 models do not cover ages younger than 1 Myr

Different ages have been estimated for Orion. Hillenbrand (1997) found that the ONC as a whole has a mean age of 0.8 Myr and an age spread of less than 2 Myr, with most SF occurring 0.3-2 Myr ago with a small tail out to 10 Myr. DM97 tracks show that 50% of the SF has occurred in the last 0.5 Myr and 85% within the last 2 Myr, therefore adopting an average of 1 Myr seems appropriate when estimating masses. However, there is also evidence that previous episodes of SF have occurred, e.g. Slesnick et al. (2004) find a distinct older population at ~ 10 Myr. Palla & Stahler (1999) also found a low level of SF 10 Myr ago, after which it accelerated to the present epoch and that the best fit age is 2 Myr. Luhman et al. (2000) find a median age for the Trapezium of 0.4 Myr for spectral types as late as M6 using DM97 models. For a discussion of sources of error and the associated problems of disentangling errors in observation and theoretical calculations from true variations in age and age spread within young clusters, see Hillenbrand, Bauermeister & White (2007).

Palla et al. (2005) studied a sample of 84 low-mass stars in the range $0.4-1 M_{\odot}$, and with isochronal ages greater than ~ 1 Myr from the Hillenbrand (1997) survey with membership probability greater than 90% to investigate if sub-

solar members have had time to significantly deplete their initial Li content. For the subsample with $M < 0.6 M_{\odot}$, in the case of stars with isochronal ages > 3 Myr, 4 show significantly depleted Li abundances. The derived ages of ~ 10 Myr indicate that the ONC does contain objects older than the average age of the dominant population, indicating that SF duration extends into the past, although at a reduced rate. The presence of a population with isochronal ages in excess of ~ 10 Myr has also been inferred by Slesnick et al. (2004) in their study of the very low mass stars and brown dwarf members. However, this apparently old population contains at least some objects with significant contamination from scattered light, which could lead to overestimation of the temperature and underestimation of the true luminosity (see below).

The 45 objects with identified spectral types are plotted on the HRD in Figure 4 along with isochrones from BCAH and DM97. The two sets of isochrones differ significantly in slope at late spectral types ($> M6$) with the DM97 isochrones being significantly steeper than BCAH. 23 of the 45 objects lie above the 1 Myr BCAH isochrone, while only 7 lie below the 5 Myr isochrone. This large fraction lying above the youngest isochrone implies that there are many very young objects, but their ages are not estimable from these tracks. The 1 Myr DM97 track passes through the region populated by objects with spectral types between M7 and M8 and might suggest a slightly older population, but again 19 objects lie above the 1 Myr isochrone, and only 6 objects below the 5 Myr isochrone. The fluxes were checked by constructing a similar diagram using the non-contemporaneous JHK photometry from Lucas et al. (2005) (where available). The results were found to be very similar, but with a slight tendency for sources to shift to higher luminosity and even younger ages (but by only 0.1 mag on average).

Objects earlier than M7 scatter about the 1 Myr BCAH isochrone, consistent with the many other estimates of the mean age of the cluster around 1 Myr, but the majority of the objects with types later than M7 lie above this isochrone. If the DM97 isochrones are adopted, the objects earlier than M7 tend to lie below the 1 Myr isochrone, but the later spectral types tend to lie above it. However, there are very significant selection effects in our sample, and especially at spectral types beyond M7. Our sample was selected to lie primarily within the $12.5 < H < 15$ magnitude range which should give an unbiased distribution of spectral types within that range, but at each spectral type there may be a bias towards bright or faint objects depending on the location of the isochrones within that range. The fact that we detect objects primarily above the isochrone is at least partially because we will tend to obtain better quality spectra of the brighter objects at a given spectral type, biasing the distribution. At types later than M7 we are not sensitive to the expected population of faint low mass BDs at ages of 1 Myr or more, and most objects detected are located above the isochrones with apparent ages less than 1 Myr. Similar effects are seen by Levine et al (2006) in the NGC 2024 cluster. At early M types, the bulk of the stellar population is brighter than the magnitude range of our sample, so we would expect to detect fainter, older objects of stellar mass (if they exist).

Infrared spectroscopy in Orion has confirmed the existence of a population of faint ($H > 17.5$ mag) objects with

deep water absorption bands which confirm them as very late M-type or early L-type low luminosity brown dwarfs or planetary mass objects (Lucas et al 2006). These lie below the 1 Myr isochrone indicating that a bias towards brighter objects operates on the sample discussed in this paper.

The other possible explanation, that the least massive members tend to be younger than more massive members, is unlikely to be the cause. There could however be an effect from the unreliability of isochrones at such young ages caused by the lack of a stellar birthline in the evolutionary calculations, which could lead to the models underpredicting the luminosity of very young low-mass objects. Alternatively, some of the objects located well above the isochrone could be binaries with nearly identical components.

A few apparently older objects, lying below the 5 Myr isochrones are also seen, but once possible spectral typing and luminosity uncertainties have been taken into account, there remain just one or two objects likely to be older than 5 Myr. The depth of the Na absorption in 011-027 places it close to the Chamaeleon values, but within the errors, it could also be located on the M dwarf sequence. It is therefore not conclusively either a cluster member or non-member. Four other objects lie below the 10 Myr BCAH isochrone, but three of them, 177-541, 156-547 and 030-524, have anomalously blue (I-J) colours, which are consistent with either a large age or an exceptionally young age (see below). 177-541 is located in the brightest part of the Orion bar, hence the error bars for its flux and temperature are probably underestimated, and as discussed in section 4.2, it has the spectral signatures of strong accretion.

6.2 Masses

The masses derived for objects on the H-R diagram are relatively insensitive to the age adopted, and are more sensitive to the spectral type or temperature assigned. This is because the tracks at young ages are primarily vertical (see Figure 5) so that an age uncertainty of a few Myr will lead to a relatively small uncertainty in the derived masses. The objects with spectral types in the range M4 to M7, where the instrument sensitivity permits good sampling of a wide range of ages, scatter about the 1 Myr isochrone. For this reason, and consistent with other studies cited above, we adopt an average age of 1 Myr.

Table 5 gives the masses found using BCAH98 tracks and an assumed age of 1 Myr. These masses are also compared where possible with the masses from photometry of LR00 and Lucas et al. (2005) for objects in common.

6.3 Comparison with HRD of Slesnick et al (2004)

Slesnick et al. (2004) constructed an HRD based on near-infrared spectroscopy for ~ 100 M-type LMS and BDs in the inner 5.1×5.1 arcmin of the ONC and found two distinct groups of objects: a young population with an average age of less than 1 Myr and a significant older population with an average age of ~ 10 Myr. The apparently older population constitutes a relatively uniform population across the mass range.

A similar situation is seen in Taurus where Luhman et al. (2003a) found that some sources appeared anomalously

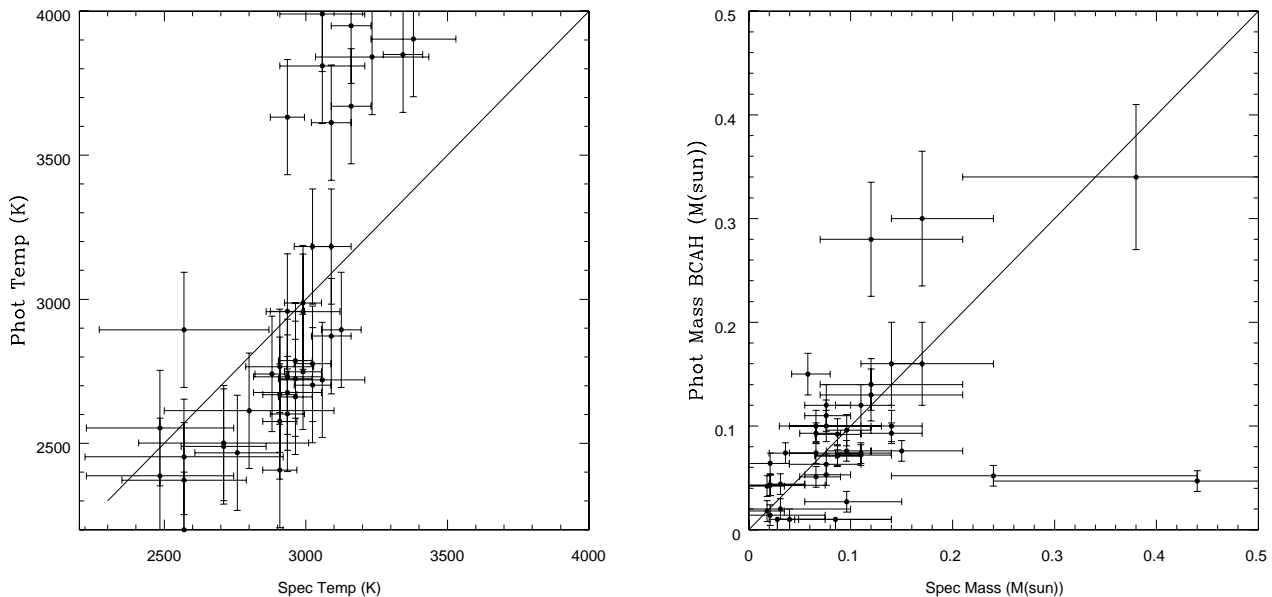


Figure 6. Left: Comparison of photometric temperatures, derived from dereddened (I-J) photometry, with the spectroscopic temperatures obtained in this work. Right: Comparison of photometric masses derived from the dereddened H-band fluxes and the BCAH 1 Myr isochrone with the masses derived from the spectral types.

old. In contrast to these results, Comeron et al. (1999) found that most of the stars in Cha I are of similar age and no significant older population is seen. Comeron et al. (2000) also found the objects to be highly clustered on the 2 Myr isochrone, suggesting an essentially coeval population having formed over a timespan of less than 1 Myr. Similarly in IC348 (1-2 Myr) and Rho-Oph (0.4 Myr), the data are consistent with very short durations for the SF (Luhman et al. 2000).

We have plotted the Slesnick et al (2004) data points together with the spectral types obtained in the current work on the HRD in Figure 5, using the same temperature scale and tracks as Figure 4. To enable direct comparison, we have calculated the dereddened H magnitudes from the data (A_V and IR photometry) presented by Slesnick et al, and used the spectral types assigned in that paper rather than the temperatures, as the temperature scale used is quite different from that in the current work. The paucity of objects older than 5 Myr in our data is in contrast to the Slesnick et al. (2004) finding of a distinct population of older objects with average ages of 10 Myr. Most of the objects in our sample are located further from the cluster centre and the dense molecular ridge of OMC-1 than the sample of Slesnick et al., so one might have expected to find older ages than in that study. The apparently old sources in the Slesnick et al. sample include only 1 or 2 objects with higher reddening than our sample (which was selected for low extinction) so the old population would not have been excluded from this study by extinction.

Slesnick et al (2004) pointed out that one of the objects in the group with ages of ~ 10 Myr is a proplyd and a further two coincide with silhouette disks. Inspection of Hubble Space Telescope (HST) $H\alpha$ data for Orion (see O’Dell & Wong 1996 and the larger Treasury dataset of Robberto et al. 2004) may resolve the discrepancy for at least a few

more of the apparently old sources. We examined the Treasury data for the 14 ‘old’ sources from Slesnick et al. (2004) (defined by spectral type $<M4$ and $K \text{ mag} > 13$) and found that 4 of them (29%) are spatially resolved with disks (3 are included in the list of O’Dell & Wong 1996). These are very young ($\ll 1$ Myr) stars surrounded by the remnants of their natal cloud cores, which are externally illuminated by the O-type stars in the centre of the cluster. We deduce that the photospheres of such sources are very strongly veiled by a combination of scattered light from the O-type stars, scattered light from the source itself and perhaps free-free emission from a stellar wind in these strongly accreting objects. This veiling would lead to overestimation of the temperature and (via an underestimate of the extinction) an underestimation of the luminosity). Furthermore, a circumstellar disk may occult the flux from the photosphere, reducing the apparent luminosity of such objects (e.g. Luhman et al 2003b). The 4 proplyd sources are numbers 25, 30, 127 and 143 from Slesnick et al. Number 127 is the well-known silhouette disc source 114-426 (McCaughrean et al. 1998).

It is possible that some of the other 10 apparently old sources in the Slesnick et al. list are also strongly veiled protostars (aged $\ll 1$ Myr) which receive insufficient ultraviolet flux from the O-type stars to be detected in $H\alpha$ imaging. In this context it is interesting to note that of the 5 ‘old’ sources detected at I band in the imaging dataset of LR00, all have anomalously blue ($I - J$) colours for their magnitudes, as defined in that work. These blue colours were attributed to scattered light, owing to an almost one to one correspondence between proplyd classification from the HST $H\alpha$ imaging and blue colour. Three of the proplyds mentioned above have I band detections and all of these have blue colours. However blue ($I - J$) colours could also be explained by a warm photosphere so it remains possible that some of these sources genuinely have ages of ~ 10 Myr.

Table 5. Effective Temperatures, Masses and Luminosities of Trapezium Objects from Spectroscopy or Photometry.

Name	Spectral Type Assigned	T_{eff} (K) Spect ^a	T_{eff} (K) Phot ^b	Mass (M_{\odot}) Spect ^c	Low M (M_{\odot})	Upp M (M_{\odot})	M (M_{\odot}) (DM97) Phot ^d	M (M_{\odot}) (BCAH98) Phot ^e	Log(L) (L_{\odot}) Phot ^f
011-027	M3.25	3380± 150	3903	0.44	0.24	0.62	0.048	0.047	-1.86
4584-117	M3.5	3343± 70	3849	0.38	0.21	0.57	0.33	0.34	-0.42
177-541	M4.25	3234± 200	3841	0.24	0.14	0.44	0.054	0.052	-1.76
112-532	M4.75	3160 ± 70	3670	0.17	0.14	0.24	0.18	0.16	-0.82
082-403	M4.75	3160± 70	3949	0.17	0.14	0.24	0.30	0.30	-0.49
091-017	M5.0	3125± 70	2894	0.15	0.12	0.21	0.087	0.076	-1.35
034-610	M5.25	3090± 70	3183	0.14	0.11	0.17	0.11	0.093	-1.17
016-534	M5.25	3090± 70	2872	0.14	0.11	0.17	0.12	0.10	-1.09
130-458	M5.25	3090± 70	3613	0.14	0.11	0.17	0.18	0.16	-0.83
121-434	M5.5	3058± 150	3990	0.12	0.07	0.21	0.15	0.13	-0.94
017-636	M5.5	3058± 150	3810	0.12	0.07	0.21	0.17	0.14	-0.88
037-246	M5.5	3058± 150	2720	0.12	0.07	0.21	0.29	0.28	-0.53
222-745	M5.75	3024± 65		0.11	0.085	0.14	0.049	0.047	-1.85
068-019	M5.75	3024± 65	2776	0.11	0.085	0.14	0.085	0.074	-1.37
019-354	M5.75	3024± 65	2702	0.11	0.085	0.14	0.081	0.072	-1.40
103-157	M5.75	3024± 65	3183	0.11	0.085	0.14	0.15	0.12	-0.97
017-710	M6.0	2990± 65	2748	0.096	0.076	0.12	0.11	0.096	-1.15
069-209	M6.0	2990± 65	2987	0.096	0.076	0.12	0.087	0.076	-1.34
156-547	M6.0	2990± 130	2957	0.096	0.055	0.15	0.033	0.027	-2.21
4559-109	M6.25	2963± 60	2787	0.087	0.065	0.11	0.082	0.072	-1.39
102-102	M6.25	2963± 60	2724	0.087	0.065	0.11	0.079	0.071	-1.42
095-058	M6.25	2963± 60	2661	0.087	0.065	0.11	0.11	0.092	-1.18
077-453	M6.5	2935± 60	3632	0.076	0.055	0.10	0.14	0.12	-0.98
072-638	M6.5	2935± 60	2958	0.076	0.055	0.10	0.055	0.053	-1.74
053-503	M6.5	2935± 120	2731	0.076	0.040	0.12	0.12	0.10	-1.10
154-600	M6.5	2935± 60	2602	0.076	0.055	0.10	0.13	0.11	-1.03
014-413	M6.5	2935± 120	2676	0.076	0.040	0.11	0.069	0.063	-1.54
4569-122	M6.75	2908± 120	2766	0.066	0.040	0.11	0.084	0.074	-1.37
035-333	M6.75	2908± 60	2576	0.066	0.05	0.09	0.11	0.093	-1.17
096-1943	M6.75	2908± 60	2669	0.066	0.05	0.09	0.053	0.051	-1.78
055-230	M6.75	2908± 180	2407	0.066	0.03	0.13	0.12	0.10	-1.12
084-305	M7.0	2880± 60	2741	0.058	0.042	0.08	0.17	0.15	-0.87
030-524	M7.5	2800± 300	2613	0.040	0.02	0.14	0.025	0.010	-2.73
217-653	M7.75	2758± 80		0.036	0.028	0.045	0.075	0.068	-1.46
042-012	M7.75	2758± 150	2467	0.036	0.020	0.066	0.083	0.074	-1.38
092-606	M8.0	2710± 300	2501	0.031	<0.014	0.10	0.029	0.020	-2.35
186-631	M8.0	2710± 150	2489	0.031	0.020	0.055	0.046	0.044	-1.90
130-053	M8.5	2570± 350	<2200	0.021	<0.014	0.075	0.045	0.043	-1.92
047-550	M8.5	2570± 350	2453	0.021	<0.014	0.075	0.026	0.014	-2.46
077-127	M8.5	2570± 220	2372	0.021	<0.014	0.040	0.069	0.064	-1.53
082-253	M8.5	2570± 300	2894	0.021	<0.014	0.055	0.044	0.043	-1.93
148-831	M8.5	2570± 350		0.021	<0.014	0.070	0.047	0.046	-1.88
183-729	M8.75	2485± 350		0.018	<0.014	0.045	0.026	0.010	-2.74
165-634	M8.75	2485± 260	2553	0.018	<0.014	0.035	0.044	0.042	-1.95
031-536	M8.75	2485± 260	2387	0.018	<0.014	0.035	0.028	0.018	-2.37

Notes:

- a) The uncertainties on the spectroscopic effective temperatures are representative errors based on the spectral type error only and do not include systematic errors in the temperature scale. At late spectral types, the quoted errors become asymmetric with the error on the low temperature side increasing to 1.5 times the value quoted.
- b) Photometric temperatures estimated from the dereddened infrared photometry. Typical uncertainties are ± 200 K (see text)
- c) Mass derived from spectroscopic temperatures and the 1 Myr BCAH isochrone. Upper and lower mass bounds are derived from the errors in the temperatures.
- d) Mass estimated from the dereddened H-band fluxes and the 1 Myr DM97 isochrone
- e) Mass estimated from the dereddened H-band fluxes and the 1 Myr BCAH isochrone
- f) Logarithm of the Bolometric Luminosity derived from the dereddened H-band fluxes (see section 5.2); the photometric uncertainties of 0.25 mag. give uncertainties of 0.1 dex in $\text{Log}(L)$.

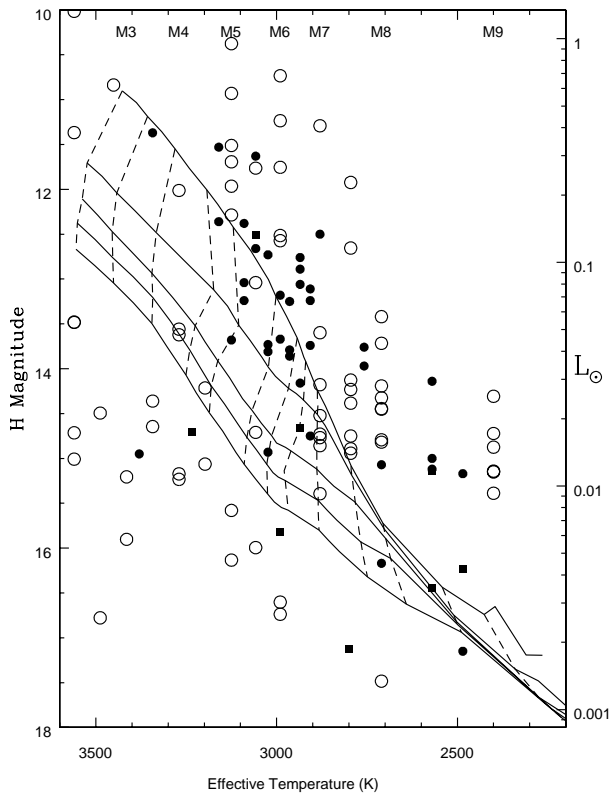


Figure 5. HRD for the data from this paper (filled symbols) together with those of Slesnick et al. (2004) (open circles). The solid lines represent the BCAH 1, 3, 5, 7 and 10 Myr isochrones while the dashed lines are the mass tracks for 0.5, 0.4, 0.3, 0.2, 0.15, 0.1, 0.08, 0.07, 0.06, 0.04, 0.03, 0.02 and 0.015 M_{\odot} from left to right.

6.4 Spectral Types and Masses from IR Data

Many of the objects in this sample have also been observed by LR00, LR01, and Lucas et al. (2005) using broad-band photometry or H and K spectroscopy. From the spectra, they defined IR water indices and compare these to the dusty model spectra of Allard et al. (2000; 2001) to derive T_{eff} and obtain spectral types from a comparison of the indices with those of local field dwarfs. Temperatures were calculated from the dereddened photometric ($I - J$) colour using the Nextgen model prediction for age 1 Myr. The uncertainties in the temperatures derived from photometry are typically ± 200 K (see LR00) (not including systematic uncertainties in the T_{eff} vs. ($I - J$) relation) but may be larger in the case of veiled protoplanetary sources. Where no photometric temperature is given, this was unobtainable due to the lack of an I band magnitude. The temperatures and masses derived from the infrared fluxes are compared with our new spectroscopic estimates in Table 5. Spectral typing errors are given in Table 2 and from these the spectroscopic temperature errors are calculated individually. Whilst a trend is present in the data in the sense that objects with higher temperatures assigned from spectroscopy are also hotter from the photometric measurements, the agreement is poor (see Figure 6a) with the photometric measurements giving much

higher temperatures for the earliest spectral types and cooler temperatures for the later types. We attribute this to errors in de-reddening, contamination by scattered light and photometric uncertainties, and believe the spectroscopically-derived temperatures to be much more reliable.

Photometric masses were derived from the luminosity vs mass relations at 1 Myr as predicted by the BCAH and the DM97 isochrones. The masses are estimated simply by matching the dereddened H-band magnitudes to the fluxes predicted by the isochrones at the distance of Orion; as discussed in section 6.2, the mass is relatively insensitive to the adopted age. The photometric masses derived from the DM97 and BCAH isochrones are quite similar, but with the former tending to give somewhat higher masses than the latter. Spectroscopic masses use the BCAH98 models assuming an age of 1 Myr. The lower and upper mass limits are calculated from the estimated spectral typing errors for each object, as listed in Table 2. In some cases, the latest possible spectral type is later than M9 where the temperature scale is not defined, so a lower limit to the mass of 0.014 M_{\odot} is quoted. The spectroscopic masses are compared with the photometric masses derived from the BCAH isochrone in Figure 6b. There is agreement overall between the two estimates, but with a number of outlying objects. The objects with significantly lower photometric masses than spectroscopic masses are those that lie below the 1 Myr isochrone in Fig 4 and, as discussed above, many have anomalous photometric colours.

The range of spectral types for this dataset is M3.25-M8.75 and at 1 Myr using the BCAH98 models these correspond to masses ranging from 0.018-0.44 M_{\odot} , i.e. from brown dwarfs just above the deuterium-burning mass limit to low-mass stars well above the hydrogen-burning mass limit. Agreement between the masses obtained from these optical spectra and those from the infrared photometric studies is variable and similar to that found by Luhman et al. (1998b) and Slesnick et al. (2004) where IR types differ by up to 3 subtypes from optical types. However, for most objects, the photometric and spectroscopic mass determinations are broadly consistent.

6.5 Binarity and its Effects on Spectroscopy & Photometry

In this study, we do not make any allowance for the effects of binaries. Although Steele & Jameson (1995) find that a photometric model of the I-band luminosity and I-K colour of artificial binary stars allowed the identification of a binary star sequence lying 0.75 mag above the single star sequence, the effect of an unresolved companion on the optical spectra would be small, shifting the spectral type by half a subclass at most. This is below the accuracy of the spectral types obtained from the spectra and therefore unmeasurable in this case. In this study, all the objects observed appear single in the images, therefore it is not possible to predict quantitatively the effects of unresolved binarity.

6.6 Mass Segregation

In such an extremely young cluster which is only a few crossing times old, we might expect that the members will not

have had time to move far from their original positions of formation so dynamical mass segregation is not yet expected to be significant (e.g. de Grijs et al, 2002), except for the most massive stars, which have become drawn to the cluster centre. There is some evidence that some mass segregation has already occurred for massive stars (Hillenbrand, 1997) but this will have a minimal effect on the low mass stars and brown dwarfs considered here.

7 SUMMARY AND CONCLUSIONS

We have obtained optical spectra of a large number of low mass stars and brown dwarfs in the Trapezium Cluster using multi-object slit masks at the AAT and Gemini-North. 45 of the objects were assigned spectral types using molecular indices which measure the strength of highly temperature sensitive molecular features (see Paper I). These indices give spectral types insensitive to the presence of nebular emission lines or imperfect dereddening. The spectra were also compared with the spectra of young Chamaeleon I objects to ensure correct spectral typing independent of luminosity class considerations. Spectral types were found to be in the range M3.25-M8.75. An additional 11 objects showed basic M type characteristics but were unable to be typed accurately due to either low S/N or veiling. Spectral types obtained at both telescopes and on different runs were found to be in good agreement.

Cluster membership probability was investigated for all 45 typed objects by an analysis of the gravity-sensitive Na absorption feature near 8200 Å. The strength of this feature was found to be much lower than that seen in older, higher surface gravity field dwarfs for all the sources except one, confirming their PMS nature and hence cluster membership. This form of evidence is extremely useful, being available and unequivocal in only moderate resolution spectra. Additional evidence was seen in the spectra of 6 objects, which showed strong CaII emission lines, indicative of accretion from a disk, also an indication of youth and hence cluster membership. The depth of the Na absorption band appears to be a sensitive tracer of age in young clusters, and higher precision measurements may prove useful in investigating the age spread in some clusters.

Spectral types were converted to effective temperatures using a temperature scale intermediate between those of dwarfs and giants, which is appropriate for young PMS objects (Luhman et al 2003b). The data were plotted on the HRD with dereddened H band magnitudes and compared with the evolutionary tracks and isochrones of Baraffe et al. (1998) and D'Antona and Mazzitelli (1997). For the majority of the sources, an average cluster age of 1 Myr was found, in agreement with several other studies. However, the majority of the lowest mass members appear younger, often residing well above the 1 Myr isochrone. While this could be a real feature of the cluster, it is more likely to be a result of selection effects in the sample observed. We find a relative lack of an apparently older population at or near 10 Myr, as found by Slesnick et al. (2004). Instead we confirm the finding of Slesnick et al (2004) that at least some of the apparently old sources are proplyds or other anomalously blue sources, and suggest that they are younger than their positions in the HRD indicate.

The results show that an average age of the Trapezium Cluster of 1 Myr is appropriate when estimating masses from photometric studies. They also show that masses estimated from photometry and spectroscopy are in generally good agreement, and MFs constructed from LFs are reliable. However, spectroscopy is still required to confirm cluster membership and to provide the most accurate estimates of mass, crucial for obtaining the true MF.

8 ACKNOWLEDGMENTS

This work is based on observations obtained at the Anglo-Australian Observatory and the Gemini Observatory, which is operated by the Association of Universities for Research in Astronomy, under a cooperative agreement with the NSF on behalf of the Gemini partnership: the National Science Foundation (United States), the Particle Physics and Astronomy Research Council (United Kingdom), the National Research Council (Canada), CONICYT (Chile), the Australian Research Council (Australia), CNPq (Brazil) and CONICET (Argentina).

We thank the Gemini and AAT Panels for the Allocation of Telescope Time for supporting this project, and the Gemini Observatory staff for carrying out Gemini observations for us. Many thanks also to Joss Bland-Hawthorn for invaluable advice and assistance before and during the AAT Taurus observations. We also thank Isabelle Baraffe for providing the theoretical isochrones.

FCR acknowledges support by a PPARC doctoral studentship and a Post-Doctoral Scholarship at Penn State University.

REFERENCES

- Allard F., Hauschildt P. H., Schwenke D., 2000, *ApJ*, 540, 1005
- Allard F., Hauschildt P. H., Alexander D. R., Tamanai A., Schweitzer A., 2001, *ApJ*, 556, 357
- Allers, K.N., et al 2007. *ApJ* 657, 511.
- Baraffe I., Chabrier G., Allard F., Hauschildt P. H., 1998, *A&A*, 337, 403 (BCAH 98)
- Bland-Hawthorn, J., Jones D.-H., 1998, *PASA*, 15, 44
- Briceño C., Luhman K. L., Hartmann L., Stauffer J. R., Kirkpatrick, J. D., 2002, *ApJ*, 580: 317
- Burrows A. et al., 1997, *ApJ*, 491, 856 (BM97)
- Close L.M., et al. 2007 *ApJ*, 660, 1492
- Cameron F., Rieke G. H., Neuhauser R., 1999, *A&A*, 343, 477
- D'Antona F., Mazzitelli I., 1997, *Mem. Soc. Astron. Ital.*, 68, 607 (DM97)
- Glazebrook, K., Bland Hawthorn, J., 2001, *PASP* 113, 197
- Gorlova N. I., Meyer M. R., Rieke G. H., Liebert J., 2003, *ApJ*, 593, 1074
- de Grijs, R., Gilmore, G. F., Mackey, A. D., Wilkinson, M. I., Beaulieu, S. F., Johnson, R. A., Santiago, B. X., 2002. *MNRAS* 337, 597
- Herbig G.H., Terndrup D.M., 1986, *ApJ* 307, 609
- Hillenbrand L.A., 1997, *AJ*, 113, 1733
- Hillenbrand L.A., Bauermeister A., & White R.J., 2007 in *Cool Stars, Stellar Systems, and the Sun XIV*, ASP

Conference Series, ed G. van Belle. In press. (astro/ph 0703642)

Hillenbrand L. A., Carpenter J. M., 2000, *ApJ*, 540, 236

Hillenbrand L.A., Hartmann L. W., 1998, *ApJ*, 492, 540

Hillenbrand, L.A., White R.J., 2004, *ApJ* 604, 741

Hirota T., 2007.PASJ in press; astro-ph/0705.3792

Kirkpatrick J. D., Henry T. J., McCarthy D. W. Jr., 1991, *ApJ*, Supplement Series, 77, 417

Kirkpatrick J. D., Henry T. J., Simons D. A., 1995, *AJ*, 109, 797

Lepine S., Rich R. M., Shara M. M., 2003, *AJ*, 125, 1598

Levine J.L., Steinhauer A., Elston R.J., Lada E.A., 2006, *ApJ* 646, 1215

Lucas P. W., Roche P. F., 2000, *MNRAS* 314, 858 (LR00)

Lucas P. W., Roche P. F., Allard F., Hauschildt P. H., 2001, *MNRAS*, 326, 695 (LR01)

Lucas P. W., Roche P. F., Tamura M., 2005, *MNRAS* 361, 211

Lucas P. W., Weights D.J., Roche P. F., Riddick F.C., 2006, *MNRAS* 373, L60

Luhman K. L., 1999, *ApJ*, 525, 466

Luhman K. L., 2004, *ApJ*, 602, 816

Luhman K. L., Briceño C., Stauffer J. R., Hartmann L., Barrado y Navascués D., Caldwell N., 2003a, *ApJ*, 590, 348

Luhman K. L., et al. 2000, *ApJ*, 540, 1016

Luhman K. L., Rieke G. H., 1998, *ApJ*, 497, 354

Luhman K. L., Rieke G. H., 1999, *ApJ*, 525, 440

Luhman K. L., Rieke G. H., Lada C. J., Lada, E. A., 1998, *ApJ*, 508, 347

Luhman K. L., Stauffer J. R., Muench A. A., Rieke G. H., Lada E. A., Bouvier J., Lada C. J., 2003b, *ApJ*, 593, 1093

Luhman K. L., Allers, K. N., Jaffe, D. T., Cushing, M. C., Williams, K. A., Slesnick, C. L., Vacca, W. D., 2007 *ApJ* 659, 1629

McCaughrean M., Chen H., Bally J., Erickson E., Thompson R., Rieke M., Schneider G., Stolovy S., Young E. 1998, *ApJ*, 492, L157

Muench A.A., Lada E.A., Lada, C.J., Alves, J., 2002, *ApJ*, 573, 366

Neuhauser R., Comeron F., 1999, *A&A* 350, 612

Osterbrock D. E., Tran H. D., Veilleux S., 1992, *ApJ*, 389, 305

O'Dell C.R., 2001, *ARA&A* 39, 99

O'Dell C.R., Wen Z. 1994, *ApJ* 436, 194

O'Dell C.R., Wong K. 1996, *AJ*, 111, 846

Palla F., Stahler S.W., 1999, *ApJ*, 525, 772

Palla F., Randich S., Flaccomio E., Pallavicini R., 2005, *ApJ*, 626, L49

Riddick F. C., Roche, P.F., Lucas, P.W. 2007, *MNRAS* submitted (paper I)

Rieke G.H., Lebofsky M.J., 1985, *ApJ* 288, 618

Robberto, M., Song, J. Mora Carrillo, G., Beckwith, S.V.W. Makidon, R. B. Panagia, N. 2004. *ApJ*, 606, 952.

Rodgers B., Wooden D.H., Grinin V., Shakhovskiy D., Natta A., 2002 *ApJ* 564, 405

Scholz A., Eisloffel J., 2004, *A&A*, 419, 249

Slesnick C. L., Hillenbrand L. A., Carpenter J. M., 2004, *ApJ*, 610, 1045

Stauffer J. R. et al., 1999, *ApJ*, 527, 219

Steele I.A., Jameson R.F., 1995. *MNRAS*, 272, 630

Wainscoat R. J., Cohen M., Volk K., Walker H., Schwartz D. E., 1992, *ApJS*, 83, 111

Wilking, B. A., Greene, T. P. Meyer, M. R., 1999, *AJ*, 117, 469

White R., Basri G., 2003, *ApJ*, 582, 1109

APPENDIX

A.1 Spectra

The 45 objects that have been classified are displayed in sequence of increasing spectral type in figure A-1. The wavelength range displayed is 6600 to 9000 Å; the spectra are contaminated by strong residual H α and [N II] emission below 6600 Å, while fringing and the falling CCD response reduces reliability above 9000 Å. The spectra have been dereddened and smoothed to a spectral resolution of ~ 10 Å, and normalised at 7500 Å. Errors in the dereddening applied will affect the slope of the spectra, but will have a smaller effect on the depth of the molecular absorption bands. Residual nebular emission lines can be seen in emission or absorption, dependent upon the local emission gradient, in some objects, while circumstellar CaII triplet emission is present in 6 objects.

Spectra of some of the objects that could not be classified reliably are shown in figure A-2. The three objects in the right panel show clear M-type spectral features, but with very strong residual nebular emission. The residual nebular emission is positive in 046-245 and negative in 196-700.

The objects in the left panel are dominated by relatively featureless continuum emission, attributed to circumstellar material, along with residual nebular emission lines and circumstellar CaII emission. These objects suffer extreme amounts of veiling. The spectra of 047-436 obtained at the AAT and Gemini are remarkable in showing substantial spectral variations. The spectral slope in the dereddened Gemini spectrum has a featureless continuum and rises to blue wavelengths, while the continuum of the AAT spectrum is redder and displays evidence of M-type features. The CaII lines go from emission in the Gemini spectrum to absorption in the AAT spectrum. Some of these differences may be attributable to the different seeing conditions at the different observatories, but it is likely that there are real spectral variations too. This type of spectral variability (correlated with photometric variations) has been observed in a more massive YSO (RR Tau) by Rodgers et al (2002). Note that in these objects, the correct amount of reddening to be applied is very uncertain. The amount of dereddening applied to 047-436, $A_V = 6.2$ mag, was derived from the photometry of LR00 and in view of the spectral variations and the circumstellar emission, must be regarded as highly uncertain. There is only a single spectrum of 117-609, and here too the reddening estimate may not be reliable.

A.2. Spectral Indices and Assigned Spectral Types

The final spectral types and associated uncertainties are listed in Table A.1 for the objects that can be classified reliably. Also shown are the spectral types given by the individual spectral indices recommended in paper I: the VO 7445 index defined by Kirkpatrick et al (1991), the VO 2

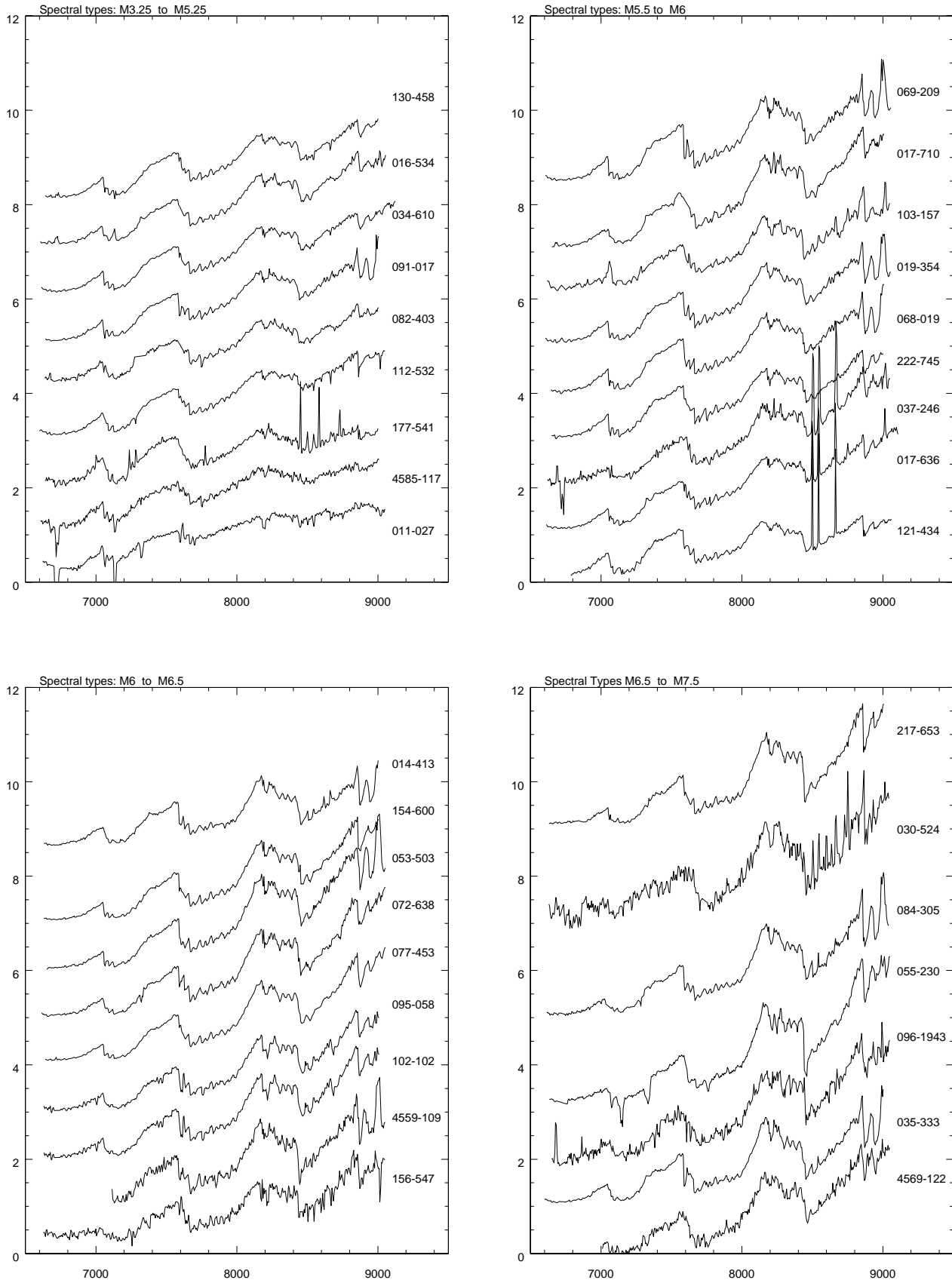


Figure A-1. The 0.66 - 0.9 μm spectra of low mass stars and brown dwarfs spanning the range of spectral types in the sample. The spectra are normalised at 0.75 μm and displaced vertically.

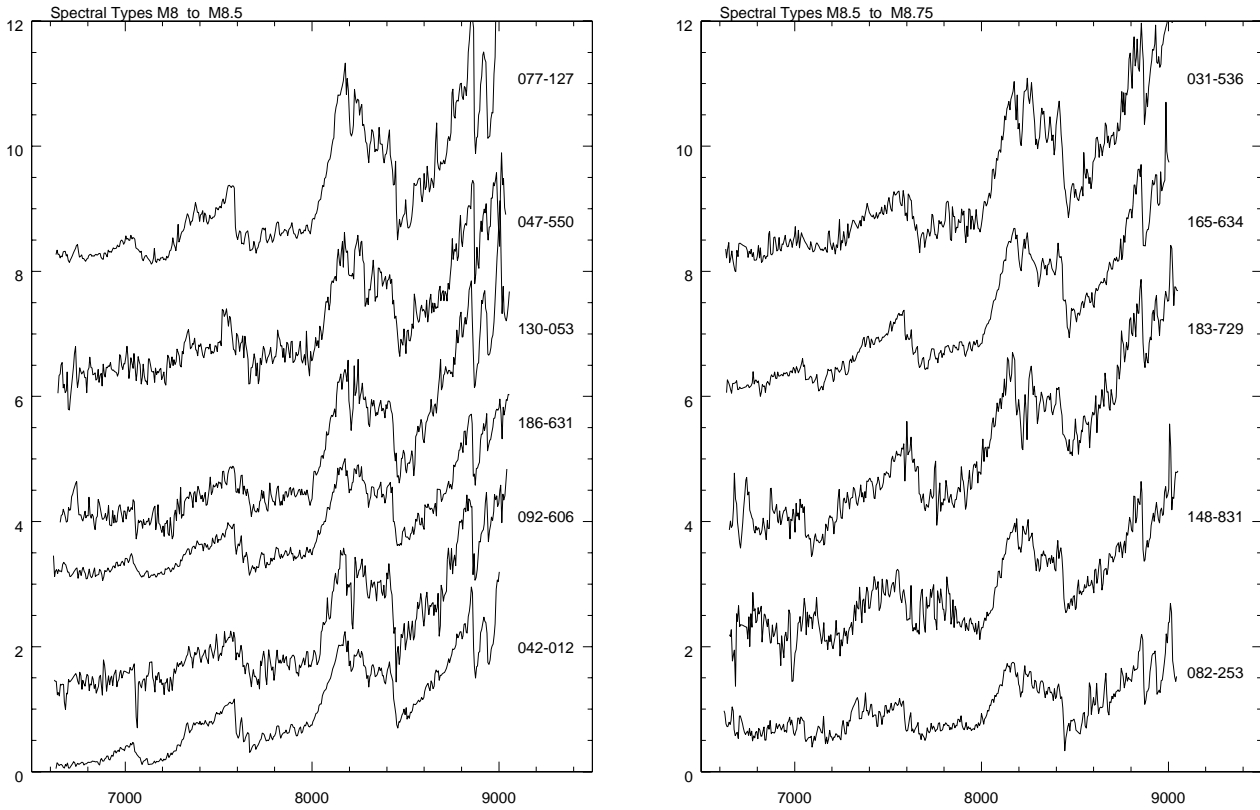


Figure A-1 continued

index of Lepine et al (2003), and the c81 index of Stauffer et al (1999). The final classifications were decided manually, taking the indices into account. The final column of the table lists the values of the Na index which provides surface gravity discrimination.

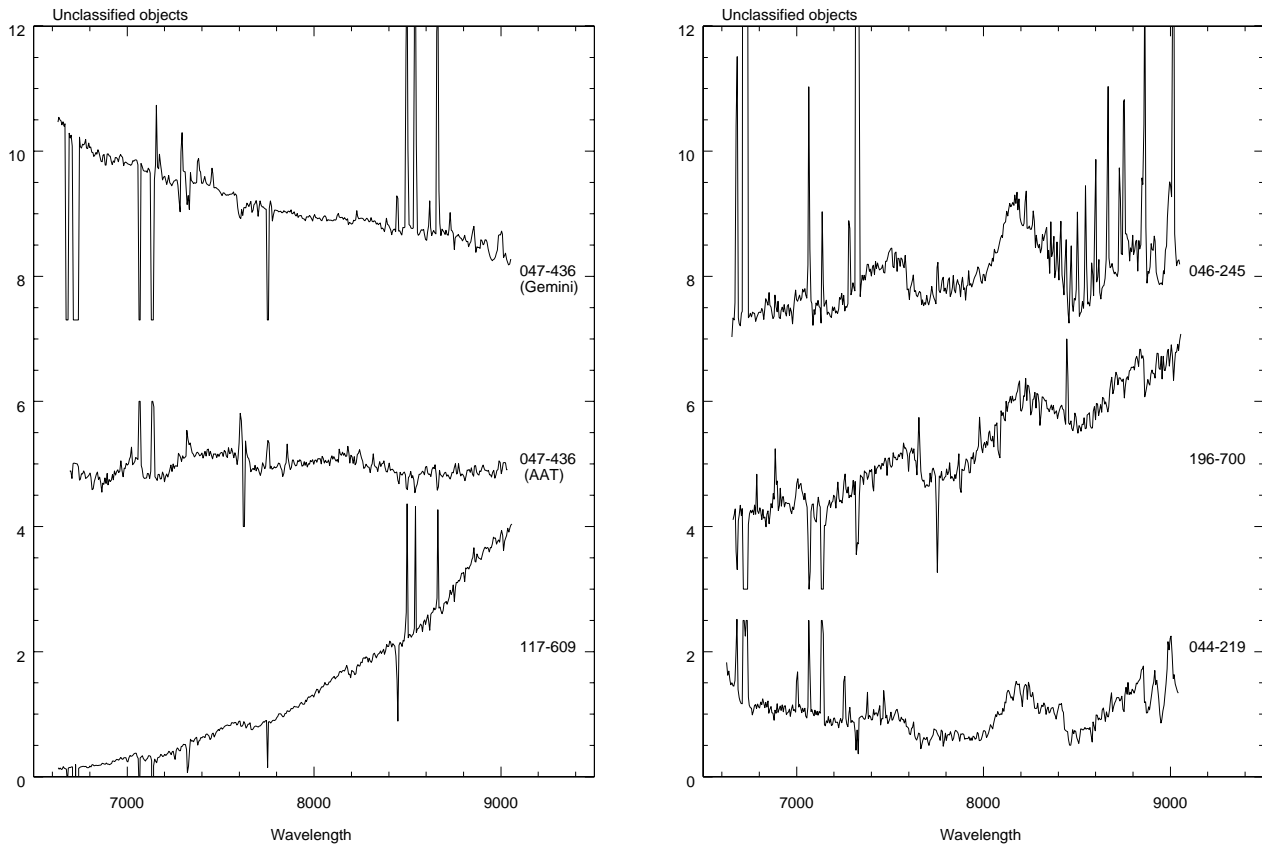


Figure A-2. Spectra of objects that could not be classified reliably. Left: 2 objects with substantial veiling and CaII emission; note that the top two spectra are of the same object taken at different epochs. Right: 3 objects with M-type features but very strong residual nebular emission

Table A-1. Spectral Types from the individual and combined spectral indices

Name	Spectral Type	Type Error	Type (VO 7445)	Type (c81)	Type (VO2)	Na Index
011-027	3.25	1.0	–	3.2	3.8	1.114
4584-117	3.50	0.5	–	3.9	4.0	1.003
177-541	4.25	1.5	–	4.4	4.3	0.961
112-532	4.75	0.5	–	4.6	5.2	1.008
082-403	4.75	0.5	–	4.8	4.8	0.980
091-017	5.00	0.5	–	4.8	5.0	0.989
034-610	5.25	0.5	5.5	5.0	5.1	0.987
016-534	5.25	0.5	5.3	5.2	5.4	0.998
130-458	5.25	0.5	5.4	5.3	5.3	0.99
121-434	5.50	1.0	5.3	4.6	5.2	0.975
017-636	5.50	1.0	5.6	3.6	4.5	0.973
037-246	5.50	1.0	<5.0	4.5	5.9	0.943
222-745	5.75	0.5	6.1	5.6	5.6	1.004
068-019	5.75	0.5	5.5	5.7	5.7	0.954
019-354	5.75	0.5	5.8	6.1	6.1	0.954
103-157	5.75	0.5	5.8	5.4	5.3	0.976
017-710	6.00	0.5	5.5	5.9	6.3	0.920
069-209	6.00	0.5	5.6	6.2	6.5	1.01
156-547	6.00	1.0	6.0	6.9	5.8	1.025
4559-109	6.25	0.5	6.5	7.0	7.0	0.92
102-102	6.25	0.5	6.6	5.9	6.4	1.01
095-058	6.25	0.5	5.5	6.4	7.8	0.93
077-453	6.50	0.5	5.9	7.3	7.0	0.919
072-638	6.50	0.5	6.7	6.3	6.8	0.934
053-503	6.50	1.0	6.7	7.3	8.3	0.97
154-600	6.50	0.5	6.2	6.6	6.7	0.931
014-413	6.50	1.0	7.6	6.2	6.6	0.91
4569-122	6.75	1.0	5.0	7.5	7.8	0.865
035-333	6.75	0.5	6.9	7.6	7.2	0.893
096-1943	6.75	0.5	–	6.7	6.8	0.881
055-230	6.75	1.5	6.5	8.4	8.4	0.86
084-305	7.00	0.5	7.1	8.1	7.9	0.871
030-524	7.50	1.5	–	7.2	7.3	0.878
217-653	7.75	0.5	7.2	8.0	7.7	0.883
042-012	7.75	1.0	7.5	8.3	7.9	0.862
092-606	8.00	2.0	7.9	–	>M8.5	0.916
186-631	8.00	1.0	7.2	8.0	8.0	0.901
130-053	8.50	2.0	–	–	–	0.72
047-550	8.50	1.5	–	9.0	>M8.5	0.829
077-127	8.50	1.0	7.9	8.4	7.4	0.808
082-253	8.50	1.5	9.0	7.7	6.9	0.96
148-831	8.50	2.0	–	–	–	0.739
183-729	8.75	1.5	–	8.3	9.1	1.015
165-634	8.75	1.0	>M8.5	–	>M8.5	0.797
031-536	8.75	1.0	>M8.5	>M8.5	8.4	0.84